Far-infrared properties of lattice resonant modes. VII. Excited states and paraelectric pairs

L. H. Greene* and A. J. Sievers
Laboratory of Atomic and Solid State Physics and Materials Science Center, Ithaca, New York 14853
(Received 24 July 1984)

Far-infrared transmission measurements have been made on single-crystal KBr:Li^+ and NaCl:Cu^+ samples up to 16 cm in length. At 1.2 K, weak satellite lines are observed at frequencies around the strong lattice-resonant-mode transition. With increasing temperature the strengths of the resonant mode and the satellite lines decrease and excited-state transitions increase in strength. Although we assume that these temperature-activated lines are excited-state transitions to the overtone levels of the resonant mode, no model potential has been found which is completely consistent with all of the infrared and Raman data. We demonstrate experimentally that these excited-state transitions can be used to monitor the mean impurity concentration of these long, inhomogeneously doped crystals. Then, using this new technique, we show that most of the satellite modes with frequencies below the resonant-mode frequency are due to impurity pairs while weak modes with frequencies near the resonant-mode frequency are associated with isolated impurities. For KBr:Li^+, a 50%-50% isotopic mixture of the dopant is used to show that the low-frequency paraelectric modes reported by Bridges arise from a diatomic Li center. Whether the center is a Li_2^+ ion or two Li^+ ions in next-nearest-neighbor sites has not been resolved.

I. INTRODUCTION

Tunneling behavior was first observed in lithium-doped KBr in 1974.[1] Subsequent investigations with the sensitive paraelectric resonance technique and with phonon spectroscopy[2] led Bridges and co-workers to propose that these paraelectric modes were associated with isolated Li^+ and that the ion was off center.[3] Such off-center behavior had been reported earlier for Li^+ in KCl where it was shown that the Li^+ impurity tunnels between a number of equivalent positions symmetrically located about the normal lattice site.[4] However, all of the early searches for tunneling levels (hence, off-center behavior) for Li^+ in KBr had yielded null results including electrocaloric effect,[5] uniaxial stress,[6] thermal conductivity,[7] and specific heat.[8] Because each of these techniques could readily detect 10^{18} impurities/cm^3 at frequencies below 10 cm^{-1}, and because no low-lying modes were observed, it had been concluded that Li^+ in KBr was on center.[9] Since both on-center and off-center behavior have now been reported for isolated Li^+ ions and KBr, a dichotomy exists.

One purpose of this paper is to describe our systematic study of these paraelectric modes with the far-infrared Fourier transform spectroscopic techniques. By measuring the concentration dependence of the line strengths in single-crystal samples up to 15 cm in length we have been able to demonstrate that the strengths of some of these transitions vary with the square of the lithium concentration. Mixtures of the two lithium isotopes as dopant have been used to conclusively identify some of the low-lying paraelectric modes with Li^+ pairs. Our results indicate that isolated Li^+ ions do not tunnel in KBr but that Li pairs do. A brief report of this double-isotope measurement already has been given.[10]

The other purpose is to describe two new effects which have been observed in these long single-crystal samples. Although the ground-state resonant-mode transition is too strong to be used as a direct monitor of the dopant concentration of the paraelectric modes in these long, inhomogeneously doped crystals, we discovered that resonant-mode excited states could be observed at elevated temperatures because their transition frequencies are far removed from those expected for a harmonic resonant-mode system. Although we have not been able to unambiguously prove that these temperature-activated lines are excited-state transitions of the overtone levels of the resonant mode because of inconsistencies in the far-infrared and Raman data, our results show that these lines definitely arise from single-impurity resonant-mode transitions of some kind. As a single-ion probe, the transitions form a convenient marker for determining the average dopant concentration in long crystals since their strengths can be controlled with the sample temperature. Irrespective of the source of these heavily damped excited-state transitions, we show that the asymmetric absorption lines can be fit by the Fröhlich oscillator model.

At the same time that the concentration dependence of the paraelectric pair modes was being identified, we accidentally discovered weak satellite modes with frequencies near the resonant mode. The line strengths for these satellites are comparable to the paraelectric pair modes yet the temperature, concentration dependence, and the double-isotope experiments demonstrate that the satellite lines above 10 cm^{-1} are associated with isolated lithium impurities.

Our success in identifying the low-lying spectrum with paraelectric Li^+ pairs and the discovery of the satellite lines lead us to search another well-known resonant-mode system, NaCl:Cu^+, for the same kind of spectral structure. Because of the heavy Cu^+ defect mass, isotopes can

no longer be used to conclusively identify pairs; however, an excited-state transition turned out to be even easier to resolve than for the KBr:Li^+ system. No single-ion satellite lines have been observed near the resonant-mode frequency but a low-lying pair spectrum has been identified. Our experimental results indicate that these Cu^+ pairs probably will not give rise to paraelectric behavior.

In the next section we describe the special experimental techniques associated with long sample measurements. The experimental data are presented in Sec. III. First the resonant mode in KBr:Li^+ is shown to vary linearly with impurity concentration and then the paraelectric modes are shown to vary quadratically both with the resonant-mode strength and the excited-state resonant-mode magnitude. The $^6Li^+$-$^7Li^+$ isotopic mixture results confirm the pair mode assignments. Finally, the resonant-mode excited-state and pair mode spectra for NaCl:Cu^+ are treated. In Sec. IV the possible sources of the single-ion excited-state transitions are explored and the form of the diatomic Li center in the paraelectric modes is discussed. The key results are summarized in Sec. V.

II. EXPERIMENTAL TECHNIQUES

The far-infrared transmission measurements were made with a lamellar interferometer in conjunction with a liquid He^3 cooled bolometer detector.[11] Sample inserts designated to accommodate 15-cm-long samples were constructed for existing cryostats.[11,12] Most of the temperature-dependent measurements were made with a five position sample holder which was immersed in superfluid helium during the early part of a run. After the helium level dropped below the bottom of the sample chamber, heaters were used to warm the sample. The nominal sample temperature was determined from 1-k Ω carbon resistors attached to the outside of the brass pipes holding the samples. Tests made with a thermometer imbedded in a crystal showed that a sample in the far-infrared beam actually was colder than the other four samples and the external monitoring resistors. The correction factor, which is presumably caused by superfluid helium flow up the detector light pipe, was about 10% of the temperature.

The alkali halide samples were obtained from Czochralski-grown single crystals prepared by the crystal growing facilities of the Materials Science Center at Cornell. Boules up to 16 cm in length were grown in order to study the concentration dependence of the weak paraelectric modes. We found that these rectangular boules could be turned down to 1.2-cm-diameter right circular cylinders on a lathe with a tool bit shaped to cut copper. Etch pit analysis of both doped and undoped KBr crystals which had been turned down showed that doped crystals had a high dislocation density within a mm of the machined surface whereas for pure crystals the high dislocation density was found throughout the bulk. Associated with the dislocations was a broad featureless absorption in the far infrared which has an absorption coefficient $\sim 3\times 10^{-2}$ cm^{-1} in the 10-cm^{-1} frequency region. This absorption band disappeared after the sample was annealed at 640 °C.

III. EXPERIMENTAL RESULTS

A. Li^+ in KBr

The richness of the impurity-induced absorption spectrum for KBr:Li^+ is illustrated by Fig. 1. The resonant-mode absorption peak is centered at 17.7 cm^{-1} for $^6Li^+$ and 16.1 cm^{-1} for $^7Li^+$. In addition to this strong feature both isotopes show a number of weak absorption lines which occur on both sides of the main band. These mode frequencies are given in Table I. The results of our concentration and isotope studies described below show that all of the spectral lines occurring below 10 cm^{-1} are attributable to Li^+ pairs. Most of the higher frequency modes are associated with isolated Li impurity ions. In an attempt to simplify the notation in the following discussions only the weak lines below 10 cm^{-1} will be referred to as paraelectric modes while all of the weak lines may be called satellite modes.

Inspection of Fig. 1 and other data show that the absorption strengths of the paraelectric modes are from 300 to 1000 times weaker than that of the resonant mode and that the strengths of both kinds of modes cannot be compared directly in a given sample length. This large disparity in strength is the fundamental experimental problem in the characterization of the paraelectric modes.

1. Concentration dependence of the resonant mode

Since one of Bridges's proposals[3] was that the resonant mode itself may be, in fact a pair mode, our first step was to measure the concentration dependence of this mode over 2 orders of magnitude. Depending upon Li concen-

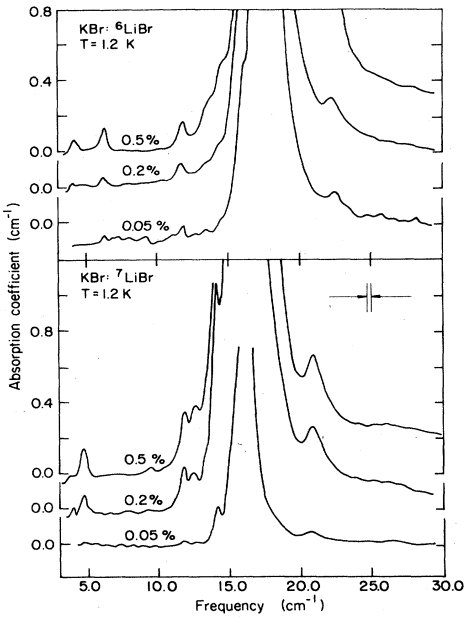

FIG. 1. Impurity-induced absorption spectra for the two isotopes of lithium-doped KBr. The lithium concentrations in mol % are given in the figure. In each case the strong resonant-mode absorption is surrounded by weak absorption lines. The instrumental resolution is 0.2 cm^{-1}. The uncertainty in the ordinate zero is ±0.1 cm^{-1}.

TABLE I. Frequencies of resonant-mode and satellite absorption lines in isotopic mixtures of KBr:Li^+.

This work (cm^{-1})			References 1 and 3 (cm^{-1})	
^6Li	^6Li-^7Li	^7Li	^6Li	^7Li
22.4*A*	22.4*A*			
	20.8*A*	20.8*A*		
17.7*B*	17.7*B*			
	16.1*B*	16.1*B*		
14.2	14.2	14.2		
13.5*C*	13.5*C*			
	12.5*C*	12.5*C*		
11.75	11.75	11.75		
6.3*D*	6.3*D*		6.5	
	5.5*D*		5.57	5.37
	4.8*D*	4.8*D*		4.7
4.2*E*	4.2*E*		4.23	4.3—5.0
	3.6		3.43	
	3.25*E*			3.2
2.95*F*	2.95*F*		2.9	
	2.6			
	2.2*E*	2.2*E*	2.3—2.7	2.2
				2.0—2.2
				1.7—2.2

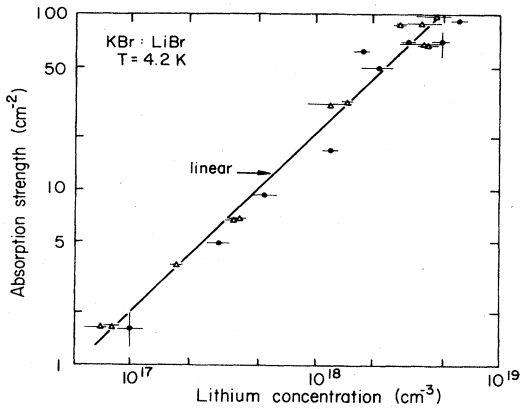

FIG. 2. Resonant-mode absorption strength versus lithium concentration at 4.2 K. The triangles are for $^6Li^+$ and the solid circles are for $^7Li^+$. The solid line is drawn through the $^6Li^+$ data. The lithium concentrations of the KBr:^{6}LiBr and KBr:^{7}LiBr samples were obtained from atomic absorption and flame emission spectroscopy. The large scatter at high concentration shows that the Li^+ resonant-mode concentration depends to some extent on sample preparation techniques.

tration the sample lengths ranged from 0.02 to 0.4 cm. The thinnest samples were produced by gluing with General Electric 7031 varnish cleaved slices onto a pure KBr substrate and sanding to the desired thickness. The absorption strength of the resonant mode of each slice was measured at 4.2 K. These slices were then chemically analyzed by atomic absorption and flame emission spectroscopy in order to extract the absolute lithium concentration. The resultant resonant-mode strength versus measured lithium concentration for the two isotopes are shown in Fig. 2. The solid line on the log-log plot with slope equal to 1 has been drawn through the $^6Li^+$ data. A similar line can be drawn through the $^7Li^+$ data. The lithium concentration error bars in Fig. 2 represent uncertainties reported in the chemical analysis. The vertical error bars, denote uncertainty in the calculation of the resonant-mode absorption strength, S_r, and arise mainly from the difficulty in measuring the sub-mm sample lengths. We conclude that the resonant-mode strength varies linearly with the Li concentration and that

$$\left.\begin{matrix} N(^6Li^+) \\ N(^7Li^+) \end{matrix}\right\} = \left\{\begin{matrix} 4.8\pm0.5 \\ 5.5\pm0.5 \end{matrix}\right\} \times 10^{16} S_r \text{ cm}^{-3} , \quad (1)$$

where S_r is measured in cm^{-2}.

This detailed analysis of different boule slices has enabled us to map out the Li^+ concentration gradient down a number of boules. We find that the amount of Li^+ in the bottom of the boule is typically 5 to 10 times larger than the top and the top 50 to 100 times smaller than what is placed in melt.

2. Concentration dependence of the paraelectric modes

a. Comparison with resonant mode. Because the 15-cm-long crystals required to observe the paraelectric modes contained a large concentration gradient, an involved procedure was required to determine the concentration dependence of these modes with respect to the resonant mode.

First, the absorption strength of each paraelectric mode $\langle S_p \rangle$, was obtained from the ratio of far-infrared transmission spectra of the doped to the undoped crystals at $T = 1.2$ K. The $\langle S_p \rangle$ values were obtained by measuring the areas under the absorption peaks with a planimeter.

Next, the lithium concentration of each long piece was determined by measuring the absorption strength of the resonant mode at several points down the boule length and obtaining an average value. The resonant-mode absorption strength $\langle S_r \rangle$ in cm^{-2} is related to the average lithium concentration by Eq. (1). If the paraelectric mode strength depends on the square of the Li^+ concentration then for samples with concentration gradients, $\langle S_p \rangle > \langle S_r \rangle^2$ and the mode strengths will not vary exactly as the square of the average concentration.

The concentration dependence of the low-frequency modes in KBr:^{6}LiBr and KBr:^{7}LiBr are shown in Fig. 3. In Fig. 3(a) the absorption strength of the 11.75-cm^{-1} mode is linear in the average concentration while the other three modes appear to follow a quadratic dependence. The situation is less clear in Fig. 3(b). Both modes appear to follow a quadratic dependence although the results for the 4.8-cm^{-1} mode are less convincing. The fact that the data for one mode produce less scatter than for the other is unusual since the absorption strengths for both modes were derived from the same far-infrared-absorption spectra. In the lowest concentration boule subsequent runs of the same sample produced different absorption strengths for the 4.8-cm^{-1} line. The three vertically connected data points in Fig. 3(b) all represent measurements on the same sample on different days. Consistent with a quadratic dependence, the 2.2-cm^{-1} mode was not observable at

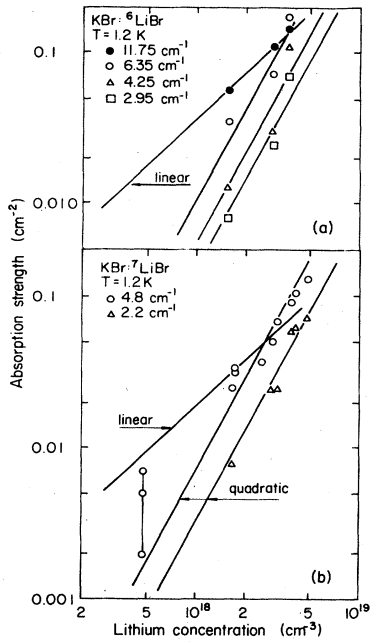

FIG. 3. Concentration dependences of the absorption strengths of some weak lines in lithium-doped KBr. (a) The three lowest frequency lines for isotopically pure ^{6}LiBr vary in strength with the square of the concentration whereas the transition at 11.75 cm^{-1} shows a linear concentration dependence. (b) The two lowest frequency lines for isotopically pure ^{7}LiBr appear to vary in strength with the square of the concentration. The scatter in the 4.8-cm^{-1} line data at the lowest concentration indicates that the strength depends on the sample history. The mode at 11.75 cm^{-1} is not plotted here because its nearness to the 16.1-cm^{-1} resonant-mode wing introduces large errors.

this low concentration.

b. Comparison with a Li^+ excited-state transition. When the sample temperature is increased from 1.2 K, both the weak modes and the Li^+ resonant mode decrease in strength and a broad absorption band increases in strength. This evolution with temperature is shown in Fig. 4, where absorption coefficient difference spectra for KBr:^{6}LiBr between 1.2 K and a larger temperature are displayed. The final temperatures which range from 3.7 K (a) to 19.5 K (e) are given in the caption of Fig. 4. A negative $\Delta\alpha$ indicates that the absorption coefficient is larger in the high-temperature spectrum than at 1.2 K. The dashed interval in the figure center identifies the frequency region where the sample is opaque because of the strong resonant-mode absorption.

Figure 4 brings out three important points.

(1) As the temperature increases the resonant mode width increases.

(2) The resonant-mode absorption is superimposed on top of a broad absorption band which is nearly frequency independent for frequencies greater than 8 cm^{-1}. This separation is most clearly seen in trace (c). The additional high-temperature absorption above 30 cm^{-1} in (c), (d), and (e) may stem from intrinsic multiphonon difference band processes.

(3) The strength of the broadband absorption is much

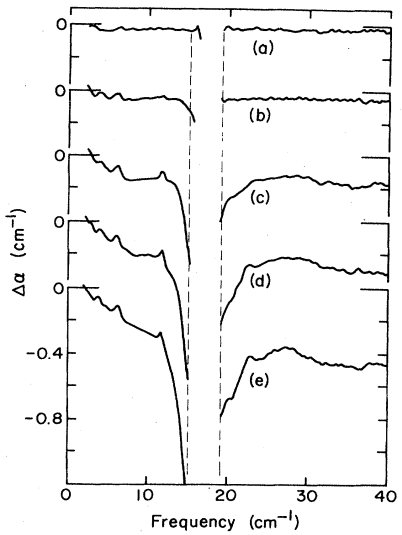

FIG. 4. Temperature-induced absorption coefficient difference spectra for KBr:^{6}LiBr. The ordinate is $\alpha(1.2\text{ K})-\alpha(T)$. The temperature for each trace is as follows: (a) 3.9 K, (b) 5.5 K, (c) 9.9 K, (d) 14 K, and (e) 20 K. For this sample length of 2.28 cm, the crystal is opaque in the frequency interval between the dashed lines. The instrumental resolution is 0.4 cm^{-1}.

larger than the strengths of the satellite absorption lines which can also be seen in this figure. This last observation leads us to propose that the broad absorption band is associated with an excited vibrational state of the $^6Li^+$ defect.

The temperature-induced change in the absorption coefficient for KBr:$^7Li^+$ was measured on a 13-cm-long crystal and the results are shown in Fig. 5. Some features in these spectra are similar to those described for the other isotope in Fig. 4. The difference between the two is that

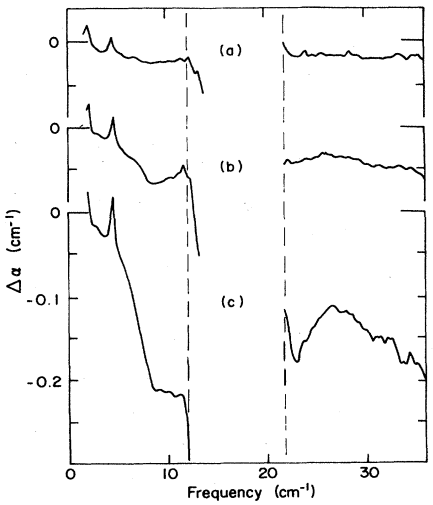

FIG. 5. Temperature-induced absorption coefficient difference spectra for KBr:$^7Li^+$. The ordinate is the same as in Fig. 4 and the temperature for each trace is as follows: (a) 3.9 K, (b) 5.5 K, and (c) 9.9 K. For this sample length of 13 cm, the crystal is opaque in the frequency interval between the dashed lines. The instrumental resolution is 0.45 cm^{-1}.

TABLE II. Far-infrared and Raman-active resonant-mode transitions at low temperature. The predicted excited-state transitions are given in the fifth column. The (0→1) lines from Ref. 9, the (0→2) NaCl:Cu^+ from Ref. 13, and the (0→2) KBr:Li^+ from Ref. 14. Frequencies are given in cm^{-1}.

System	Far infrared (0→1)	Raman (0→2)	Irreducible representation	Far infrared (1→2) Calculated	Measured
KBr:$^6Li^+$	17.7		T_{1u}		
		28	E_g	10.3	8.0
		40	A_{1g}	22.3	
KBr:$^7Li^+$	16.1		T_{1u}		
		27	E_g	10.9	8.8
		38	A_{1g}	21.9	
NaCl:Cu^+	23.5		T_{1u}		
		40,62.5	E_g	16.5,39.0	15.0
		48	$A_{1g}+T_{2g}$	24.5	

the broad absorption band can no longer be characterized as frequency independent. Two features stand out in the temperature-induced absorption, one at a frequency of 8.8 cm^{-1} and the other at 23 cm^{-1}.

To see if these excited-state transitions correspond to transitions to resonant-mode overtone states, we compared our results with those obtained from the measured ir-[9] and Raman-[13,14] active modes which are listed in Table II. The frequencies measured here (column 6) differ from those calculated (column 5) by about 2 cm^{-1} in each case. Also, it is even less clear for $^6Li^+$, that the excited-state absorption is related to the resonant-mode excited state since the Raman scattering measurements give well-defined lines[14] while no lines can be seen in Fig. 4. We shall analyze these excited-state spectra in more detail in Sec. IV and the conclusion will be that this broadband absorption is probably caused by a resonant-mode excited-state transition.

Once the excited-state absorption band has been assigned to a single Li^+ ion vibrational mode, monitoring the paraelectric mode strength as a function of Li^+ concentration becomes quite straightforward. Figure 6 shows the impurity-induced temperature-dependent absorption coefficient in the low-frequency region for the two isotopes. By taking the difference of a KBr:Li^+ absorption spectrum at 1.2 K with a second one at 5.5 K then according to Fig. 6 for this particular impurity concentration the paraelectric modes and the broad excited-state transition at the frequency identified by the dashed line have opposite sign but roughly equal magnitudes for this spectral resolution of 0.44 cm^{-1}. For a fixed temperature difference a comparison of the relative heights of the two contributions for different Li^+ concentrations can be made with increased precision over the technique of comparing the strengths of the paraelectric modes to that of the resonant mode itself. To be more precise the areas of the two kinds of transitions should be compared, not the heights, since both the resonant-mode and paraelectric mode linewidths depend to some extent on impurity concentration; however, the absence of a well-defined linewidth for the broad excited-state transition shown in Fig. 6 makes this approach impractical.

From absorption spectra like those in Fig. 6 (but at a resolution of 0.1 cm^{-1} so that the modes are resolved) the relative concentration dependence of the satellite modes for the ^{6}LiBr isotope has been determined and the results are shown in Fig. 7. For each line the difference in the absorption coefficient is plotted versus the difference in the excited-state absorption value at 8 cm^{-1} for a temperature change from 1.2 to 5.5 K. The figure shows that the 11.75-cm^{-1} line varies linearly with LiBr concentra-

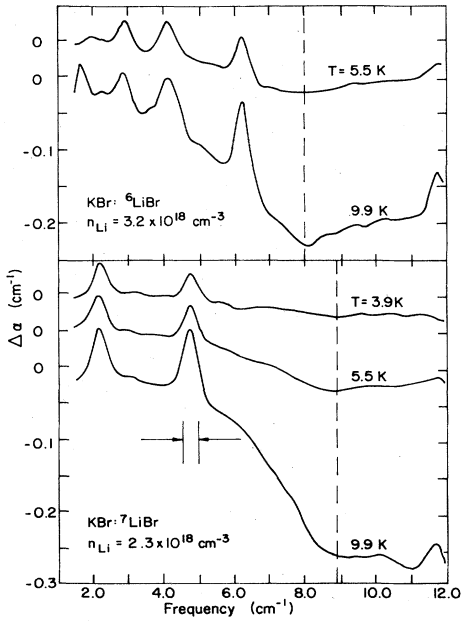

FIG. 6. Temperature-induced absorption coefficient difference spectra at low frequencies for KBr:^{6}LiBr and KBr:^{7}LiBr. The reference spectrum is at 1.2 K. The impurity concentrations are given in the figure. The height of the temperature-dependent excited-state absorption at the dashed marker for a fixed temperature is used for a relative calibration of the isolated Li^+ concentration from sample to sample. The resolution is 0.44 cm^{-1}. Note that the modes are not resolved at this resolution.

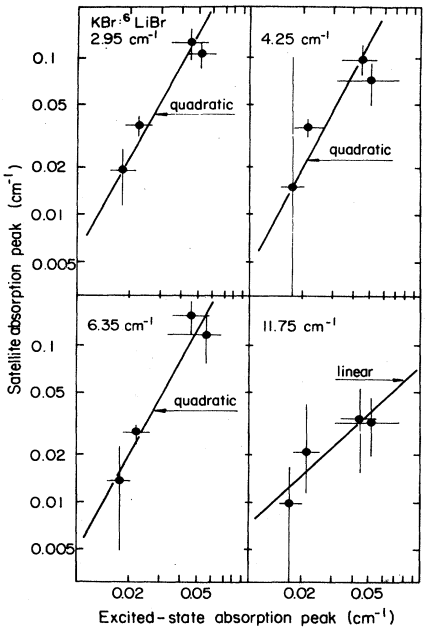

FIG. 7. Satellite peak height vs excited-state peak height for different $^6Li^+$ concentrations. The largest concentration is smaller than that shown in Fig. 6. The comparison is made for a temperature change from 1.2 to 5.5 K. The broadband height is measured at 8 cm^{-1}. The paraelectric modes exhibit a quadratic dependence while the 11.75-cm^{-1} line is linear in the lithium concentration. The resolution is 0.10 cm^{-1}.

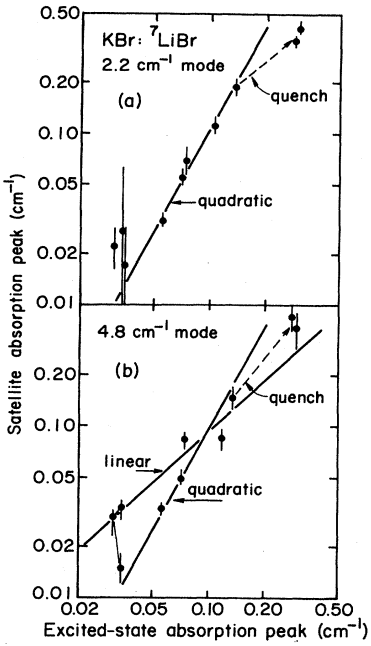

FIG. 8. Satellite peak height vs excited-state peak height for different $^7Li^+$ concentrations. (Same temperature change as Fig. 6.) The broadband height is measured at 8.8 cm^{-1}. Both paraelectric modes appear to follow a quadratic concentration dependence. The three lowest concentration data points in (b) which are connected by a solid line were obtained from the same sample on different days. The changes indicate that this absorption band depends on sample history. The large scatter in the 4.8-cm^{-1} data indicates that another type of impurity mode may be near by in frequency. As noted in the figure, quenching the crystal from high temperature enhances the strengths of both the satellite modes and the single-ion excited-state mode. The resolution is 0.10 cm^{-1}.

tion while the three paraelectric modes show a quadratic concentration dependence. These results are the same as those found in Sec. III A 2 a but now the experimental uncertainties are reduced.

The experimental results for the ^{7}LiBr isotope are shown in Fig. 8. The concentration dependence is not as clear as for the lighter isotope. In particular, for the 4.8-cm^{-1} absorption line the data are fit almost equally well with a linear or quadratic dependence. The 11.75-cm^1 line which is not shown is again linear in concentration but since no isotope effect is observed this mode is attributed to an unwanted impurity in the LiBr dopant.

We find that either quenching the crystal from 350 °C or annealing it increases the strength of both the satellite modes and the resonant-mode excited state. Quenching was accomplished by raising the temperature of a sample is an evacuated, sealed quartz ampoule to at least 350 °C and then cooling it to room temperature in a few min. Upon performing this experiment on KBr:^{7}LiBr, roughly a factor of 2 enhancement, both in the satellite and in the excited-state resonant absorption peaks, was found. Results of this experiment are denoted by the dashed arrow labeled "quench" in Figs. 8(a) and 8(b) which connect data points obtained from the same crystal before, and after, quenching. A similar enhancement was also found when the sample was annealed. These results are different from those reported by Russell and Bridges[3] where quenching from 650 °C produced orders of magnitude enhancement of the satellite modes. Their, Li^+ concentration was about a factor of 10 smaller than ours.

Russell and Bridges[3] also found that the addition of OH^- to KBr:Li^+ strongly suppressed the pair modes. We have confirmed this result for both diffusion doped and Czochralski-grown crystals. Our new result is that the single-ion resonant mode is suppressed as well. This was convincingly demonstrated by measuring the low-temperature spectrum of a Czochralski-grown crystal of KBr + 0.1 mol %K ^{6}LiOH which was 12-cm long. Instead of a resonant mode at 17.7 cm^{-1} with $\alpha_{max} \sim 8$ cm^{-1}, a weak ($\alpha_{max}=0.05$ cm^{-1}) broadband [full width at half maximum (FWHM) of 10 cm^{-1}] was observed at 15 cm^{-1}. No satellite modes were detected. Subsequent chemical analysis revealed that the lithium concentration of this sample ranged from $n_{Li}=7.3\times10^{17}$ cm^{-3} up to $n_{Li}=1.6\times10^{18}$ cm^{-3}. A measurement of the near-infrared spectrum showed that $LiOH^-$ remains as a molecule in the KBr host.

3. *Identification of paraelectric modes with isotopic mixtures*

Because of the history dependence of some of the paraelectric modes the cleanest experiment for distinguishing between single ion and pair modes has been to

measure the spectrum of a KBr crystal grown with equal mole percentages of ^{6}LiBr and ^{7}LiBr dopants. If pair modes are important then in such a crystal 25% of the centers will be $^6Li^+$ pairs; 25%, $^7Li^+$ pairs; and the remaining 50%, $^6Li^+$-$^7Li^+$ pairs.

Three broadband absorption spectra for different isotopic mixtures of Li^+-doped KBr are shown in Fig. 9. The concentrations placed in the melt are given in the figure caption. In order to view weak modes, sample lengths again have been chosen so that the crystals are opaque in the resonant-mode frequency region. Absorption spectra over this frequency range for different concentrations of isotopically pure Li-doped KBr have already been presented in Fig. 1. Above 10 cm^{-1}, the weak absorption peaks observed for the isotopically pure dopants, curves (a) and (c), can also be seen in the combination dopant curve (b). With a thinner combination crystal the two resonant modes can be resolved. The center frequency of each of these absorption lines in the double-doped crystal is recorded in Table I. Most interesting, however, is the frequency region below 10 cm^{-1}, where absorption lines appear in the combination crystal at frequencies which do not correspond to the lines observed in the spectra for isotopically pure dopants. The combination modes are most easily seen in Fig. 10 where high-resolution spectra below 10 cm^{-1} are shown for KBr with different isotopic mixtures of Li^+ dopant. The concentrations of $^6Li^+$ [curve (a)] and $^7Li^+$ [curve (c)] are measured spectroscopically to be about the same: $\sim 3\times10^{18}$ cm^{-3}. The 50%-50% isotopic mixture [curve (b)] is the same crystal that was shown in Fig. 9. If the absorption lines in trace (b) of Fig. 10 were associated with isolated Li^+ ions then the resultant would be a simple sum of curve (a) and curve (c);

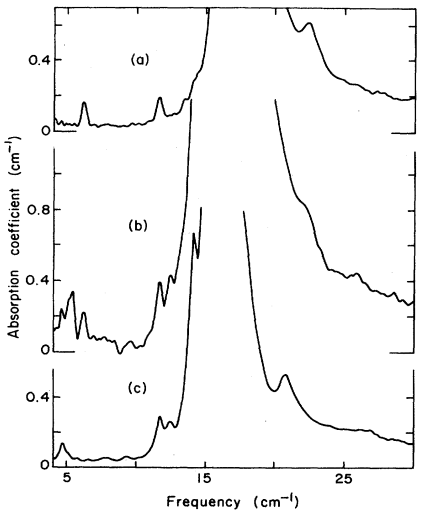

FIG. 9. Impurity-induced absorption spectra from 4 to 20 cm^{-1} for different isotopic mixtures of Li-doped KBr. The sample temperature is 1.2 K and the instrumental resolution is 0.2 cm^{-1}. The dopant concentrations in the melt are as follows: curve (a) KBr + 0.2 mol % ^{6}LiBr, curve (b) KBr + 0.25 mol % ^{6}LiBr + 0.25 mol % ^{7}LiBr, and curve (c) KBr + 0.2 mol % ^{7}LiBr. All of the absorption lines in curves (a) and (c) also occur in curve (b); however, a new absorption line appears in curve (b) at 5.5 cm^{-1}.

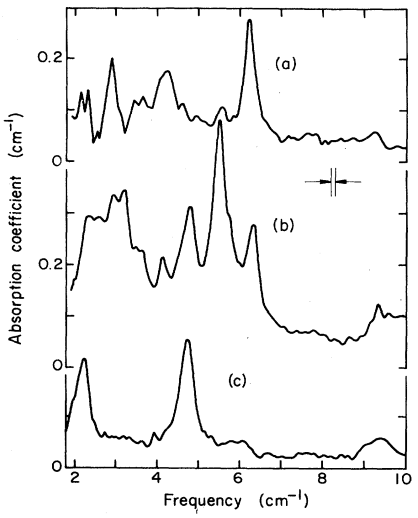

FIG. 10. Impurity-induced absorption spectra from 2 to 10 cm^{-1} for different isotopic mixtures of Li-doped KBr. The sample temperature is 1.2 K and the instrumental resolution is 0.1 cm^{-1}. The dopant concentrations are as follows: curve (a) 3×10^{18} cm^{-3} ^{6}LiBr, curve (b) is the same as curve (b) in Fig. 9, and curve (c) 3×0^{18} cm^{-3} ^{7}LiBr. Note that new modes appear in the combination crystal spectrum [curve (b)] which are not seen in curves (a) or (c).

however, if the modes are due to dynamically coupled Li^+ pairs, then new modes should appear when the two isotopes are mixed. Inspection of Fig. 10 demonstrates that the isolated ion model cannot account for curve (b). The three highest frequency modes are clearly identifiable with pairs because the new strong line in curve (b) at 5.5 cm^{-1} does appear to be about twice as strong as the 6.35 cm^{-1} ($^6Li^+$-$^6Li^+$) and the 4.8 cm^{-1} ($^7Li^+$-$^7Li^+$) lines. Moreover, the frequency of this new combination mode is halfway between the frequencies of the other two modes. The actual absorption strengths of these three modes are uncertain because of band overlap. Within these uncertainties the $^6Li^+$-$^6Li^+$- and $^7Li^+$-$^7Li^+$-induced absorptions are of equal strength and each half as strong as the $^6Li^+$-$^7Li^+$-induced absorption. All of these line centers are recorded in Table I. The zero-field paraelectric mode frequencies measured by Bridges and Russell,[1,3] are also listed in this table for reference.

Before considering the more complex part of curve (b) in the 3-cm^{-1} region, it is helpful to review how the isotope effect can be used to characterize the mode type. The identification is shown in Fig. 11, where the center frequencies are given for the different isotopic combinations of the dopant. The resonant mode is labeled by the letter *B*. One mode is observed for the isotopically pure dopant and two modes for the 50%-50% mixture, similarly for the other high-frequency modes. Points $D(6)$ and $D(7)$ identify the highest frequency modes in the pair mode spectrum for two isotopically pure dopants. The dashed line connecting these two points indicates the position where the new combination mode appears with double the strength. Data points $E(6)$ and $E(7)$ identify the

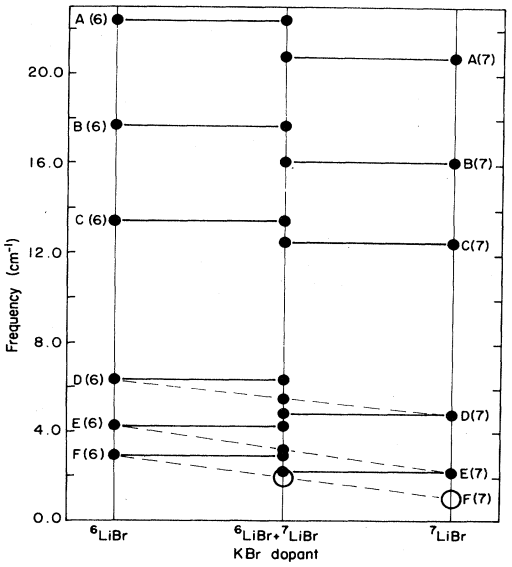

FIG. 11. Absorption center frequencies vs Li isotopic mixture for modes exhibiting an isotope shift in KBr:LiBr. The solid circles identify measured frequencies for each of the three combinations of isotopes. The capital letters next to the solid circles identify modes of the same type. Modes *A*, *B*, and *C* are due to isolated ions while *D*, *E*, and *F* are due to Li pairs. The dashed lines cross the 50%-50% isotopic mixture value at the frequencies observed for the new combination lines. Open circles are predicted modes.

next two highest frequency modes and the dashed line indicates where the combination mode is expressed for a 50%-50% isotopic mixture. The solid circle indicates that a strong mode does exist at this position. The closeness of the $F(6)$ absorption line to this frequency produces the other major feature in the complex spectrum. It has not been possible to observe the $F(7)$ line since it is below the range of our instrument but the relative strength of $F(6)$ to $E(6)$ remains unchanged in crystals of different Li concentrations. We conclude that all of these paraelectric modes are associated with Li pairs. Because the combination lines occur halfway between the pure isotope lines the Li's must be strongly coupled to each other.

B. Cu^+ in NaCl

1. Resonant-mode excited states

The Cu^+-induced spectrum in NaCl is characterized by a strong infrared-active mode at 23.5 cm^{-1} and weak satellite lines at lower frequencies. This satellite structure is shown in Fig. 12 for 0.2 and 0.5 mol% CuCl dopant in the melt. The satellite center frequencies are at 9.8, 15.8, 17.5, and 18.3 cm^{-1}.

In order to estimate the Cu^+ concentration dependence of the satellite modes we have identified the excited-state vibrational spectrum of the Cu^+ defect. The dotted trace in Fig. 13 is the temperature-induced absorption spectrum $[\alpha(1.2\text{ K})-\alpha(9.9\text{ K})]$ of a 0.05 mol% CuCl-doped NaCl crystal which is 16.3 cm long. As temperature is increased the absorption band centered at 15 cm^{-1} grows in strength indicative of an excited-state transition.

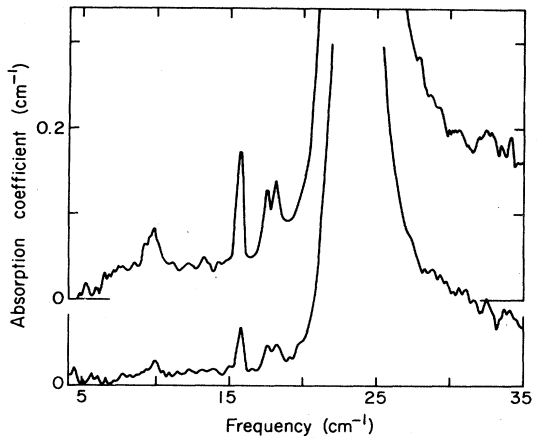

FIG. 12. Impurity-induced absorption spectra for two concentrations of Cu^+ in NaCl. Top trace: 0.5 mol% CuCl in the melt. Bottom trace: 0.2 mol% CuCl in the melt. The increase in noise above 25 cm^{-1} occurs because of the small intensity in this frequency region. Weak absorption lines occur on the low-frequency side of the strong resonant mode. The frequencies are given in the text. Instrumental resolution is 0.2 cm^{-1}.

Raman scattering measurements by Ganguly *et al.*[13] show that two even parity resonances occur in this frequency region. The frequencies and assignments are given in Table II. If the Raman transitions are identified as components of the $0\rightarrow2$ resonant-mode overtone transitions then the ir-active $1\rightarrow2$ transitions would occur at 16.6 and 24.6 cm^{-1}, respectively. The first value is 1.6 cm^{-1} larger than the frequency of the observed infrared excited-state mode while the second would be masked by

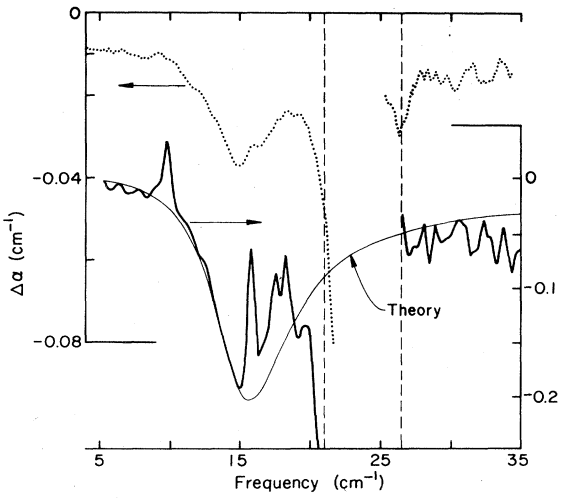

FIG. 13. Temperature-induced absorption coefficient difference spectra for two Cu^+ concentrations in NaCl. The $\Delta\alpha$ is obtained for a temperature change from 1.2 to 9.9 K. Dotted trace: 0.05 mol% CuCl in the melt. Solid trace: 0.5 mol% CuCl in the melt. The decrease in signal-to-noise ratio above 25 cm^{-1} occurs because of the small throughput in this particular arrangement. Instrumental resolution is 0.43 cm^{-1}.

the strong $0\rightarrow 1$ transition

Because a well-defined excited state has been obtained, it is possible to test the width of the observed excited-state absorption to see if it is consistent with the resonant-mode idea. For impurities which are weakly coupled to the surrounding lattice so that low-frequency resonant modes result, the linewidth is proportional to the fourth power of the mode frequency. We find that the experimental ratio of the width of the 15-cm^{-1} line to the $0\rightarrow 1$ width is 1.3 times the theoretical value of the ratio of the $0\rightarrow 2$ to the $0\rightarrow 1$ width indicating that the final state is about 40 cm^{-1} above the ground state. In addition, the growth of the 15-cm^{-1} line with temperature is consistent with the population effect for an initial state which is roughly 24 cm^{-1} above the ground state.

2. *Concentration dependence of satellite modes*

In addition to the broad excited-state transition in Fig. 13 a number of sharp ground-state transitions can also be seen. It seems unlikely that these lines correspond to tunneling modes since an isotope shift characteristic of a tunneling system is not observed. The Cu^+ dopant is two naturally occurring isotopes: 69% with mass 63 and 31% with mass 65. For the resonant-mode transition the isotope shift is 0.37 cm^{-1} which is smaller than the linewidth but for tunneling states the shift should be larger than the linewidth and asymmetric doublets should occur in the spectrum. If the Cu^+ impurities were to form paraelectric pairs as found for KBr:Li^+, then triplets would exist with relative strengths (0.47):(0.43):(0.10). From Figs. 12 and 13 any isotope shift must be smaller than 1 cm^{-1}, hence, the lines probably are not associated with tunneling transitions.

To determine the concentration dependence of these modes we compared the mode strengths with that of the excited-state transition. Because the absorption lines occur at higher frequencies in NaCl:Cu^+ than do the corresponding lines in KBr:Li^+, the comparison between the satellite and the excited-state heights were made at 9.9 K. The absorption coefficient difference as a function of frequency for four different concentrations of CuCl in NaCl (0.05, 0.02, 0.5, and 1 mol %) shows that the satellite lines vary quadratically with the Cu^+ concentration. We conclude that all of these transitions are due to Cu^+ pairs.

IV. DISCUSSION

A. Resonant-mode excited states

1. *Model oscillator potentials*

The identification of the paraelectric pairs in KBr:Li^+ and the pair modes in NaCl:Cu^+ relies fairly heavily on the assignment of an excited-state transition of the resonant mode for an isolated impurity in the same spectrum. A comparison of the temperature-induced spectra absorption coefficient at 9.9 K for KBr:$^6Li^+$ (Fig. 4), KBr:$^7Li^+$ (Fig. 5), and NaCl:Cu^+ (Fig. 13) shows that these excited-state spectra are all different. For $^6Li^+$ the spectrum is characterized by a broad featureless absorption with a shoulder at 8 cm^{-1}, for $^7Li^+$, lines at 8.8 and 23 cm^{-1} are superimposed on a broad absorption while for Cu^+, a fairly well resolved line is observed at 15 cm^{-1} superimposed on a relatively weak broadband absorption. Because these frequencies are close to those expected for excited-state transitions of the resonant mode (see Table II) we have labeled them as such throughout this work. Now we would like to make a critical review of this assignment.

In order to observe any excited-state transition at low temperature in the far infrared it must be shifted from the harmonic-oscillator value by a few cm^{-1} otherwise it would be obscured by the strong ground-state resonant-mode transition. A large fourth-order anharmonicity term in the resonant-mode potential could be introduced to account for this shift except for the fact that earlier Stark effect measurements on KBr:Li^+ have an upper limit on the magnitude of such a term in the potential which is about 50 times smaller than required to account for the observed excited-state shift.[15] To argue that these are excited-state transitions to overtone modes one must account for this discrepancy.

The large isotope effect and small Stark effect results for KBr:Li^+ have been shown to be consistent with a model in which the Li^+ potential well has displaced energy minima from the normal equilibrium lattice site but with barriers which are small compared to the Li^+ zero-point energy.[15] Such a harmonic potential with a central bump produces a large isotope effect but a small Stark effect for the ir-active resonant-mode transition.

As we now show this same potential cannot account for the E_g Raman-active overtone transition given in Table II. For a three-dimensional harmonic oscillator with a perturbing potential of the form

$$H_p = A\exp(-cr^2)\ , \tag{2}$$

the first-order perturbed transition energies are

$$\hbar\Omega_{01}(T_{1u}) = \hbar\omega - AR^{3/2}(1-R)\ , \tag{3}$$

$$\hbar\Omega_{02}(E_g, T_{2g}) = 2\hbar\omega - AR^{3/2}(1-R^2)\ , \tag{4}$$

and

$$\hbar\Omega_{02}(A_{1g}) = 2\hbar\omega + \frac{AR^{3/2}}{2}(1-6R+5R^2)\ , \tag{5}$$

where $R = M\omega/(c\hbar + M\omega)$ and M and ω are the harmonic-oscillator mass and frequency, respectively. Inspection of Eqs. (3), (4), and (5) shows that for $0 < R < 1$ the following inequalities hold:

$$2\hbar\Omega_{01}(T_{1u}) < \hbar\Omega_{02}(E_g, T_{2g}) < \hbar\Omega_{02}(A_{1g})\ . \tag{6}$$

Since the perturbed overtone transition frequencies are both larger than 2 times the fundamental transition, the potential with the central bump cannot account for the observed Raman-active E_g transition.

Analysis of the NaCl:Cu^+ Raman data has produced a possible explanation of the large overtone splitting.[13] If a Fermi resonance occurs between the overtone of E_g symmetry and an E_g symmetry resonant mode which is nearby in energy then the mixing and shifting of these two modes would produce the observed 40 cm^{-1} and 62.5 cm^{-1} modes. The best fit to the resonances is a mixture

of 65% E_g overtone and 35% E_g resonant for the low mode while for the high mode the mixtures are reversed.[13] The A_g and T_{2g} overtones retain their nearly harmonic frequencies in agreement with the experimental data. In light of the NaCl:Cu^+ analysis an obvious proposition is that a Fermi resonance for E_g symmetry resonant modes also occurs in KBr:Li^+. Although this approach could account for the 27-cm^{-1} resonance, other problems appear. First, two E_g resonances are not observed in the Raman data. Second, the T_{2g} overtone resonance is missing. Finally, it seems a remote possibility that these two very different lattice-defect systems would have accidental Fermi resonances which accomplish the same end.

Because neither the potential bump nor the Fermi resonance provide a consistent description of the far-infrared and Raman data, we are lead to consider the possibility that other degrees of freedom of the lattice-defect system may be involved. Recently, it was proposed that the KI:Ag^+ lattice-defect system had two low-lying elastic configurations each with its own Ag^+-induced vibrational spectrum.[16] The second configuration becomes populated at elevated temperatures. For KBr:Li^+ or NaCl:Cu^+ the entire low-temperature impurity-induced spectrum would stem from one elastic configuration. Nearby in energy would be a second elastic configuration in which the local lattice around the impurity would have a different equilibrium arrangement. Because the temperature-dependent properties of the low-temperature spectra for these two defect systems do not vary as rapidly as does KI:Ag^+, both Li^+ and Cu^+ would still be located at a normal lattice site in the second configuration. The Raman lines, at least for KBr:Li^+, would then simply correspond to A_{1g} and E_g resonant-mode transitions in the first configuration while the far-infrared lines which appear at elevated temperatures would be associated with the T_{1u} resonant-mode transition in the second configuration. This model would permit fairly harmonic resonant modes consistent with the small Stark effect and the frequency difference between the calculated and measured excited-state transitions listed in Table II would become irrelevant.

The problem with the two configuration model is that experimentally the temperature dependence of the population in the second configuration is consistent with an excitation energy which, within a few wave numbers, is the same as the resonant mode $0\rightarrow 1$ transition energy in the first configuration. Since there is no *a priori* reason why, in this picture, the energy of the second configuration should be so closely related to the first one, this experimental observation leads one back to considering excited states in the single configuration model again. Because of insufficient evidence to the contrary, we shall continue to assume that the single configuration model is valid for both KBr:Li^+ and NaCl:Cu^+.

2. *Asymmetric line shape*

In assigning the asymmetric absorption lines to resonant-mode excited states so far we have ignored the fact that they do not look like the Lorentzian shape of the low-temperature resonant-mode line. Van Vleck and Weisskopf[17] and also Fröhlich[18] have derived resonance expressions which are similar to the Lorentz formula in the limit of small damping but which are asymmetric and consistent with the Debye case in the large damping limit. Following their approach, the analogous procedure here is to invoke thermodynamic equilibrium between the resonant mode and the applied far-infrared electric field immediately after each phonon collision.[19] For this condition the attenuation coefficient associated with the excited-state resonant-mode transition can be written as[18]

$$\alpha=\frac{1}{2}\Delta\epsilon/(\epsilon_0)^{1/2}\frac{\Omega^2}{C}\left[\frac{\Gamma}{(\Omega-\Omega_{12})^2+\Gamma^2}+\frac{\Gamma}{(\Omega+\Omega_{12})^2+\Gamma^2}\right], \tag{7}$$

where ϵ_0 is the static dielectric constant of the list, Ω_{12} and 2Γ are the transition frequency and full linewidth in r/s, and c is the velocity of light. The quantity $\Delta\epsilon$ which depends on the population difference between the two states Δn, is defined by the following two equations:

$$\Delta\epsilon=\left[\frac{4\pi}{3}\right]\left[\frac{2}{\hbar\Omega_{12}}\right]\left[\frac{\epsilon_0+2}{3}\right]^2\Delta n\,|P_{12}|^2 \tag{8}$$

and

$$\Delta n=N[1-\exp(-\hbar\Omega_{12}/kT)][\exp(-\hbar\Omega_{01}/kT)]\times[1-\exp(-\hbar\Omega_{01}/kT)]^3, \tag{9}$$

where P_{12} is the transition dipole moment, N is the impurity number per cm^3 and the last term in Eq. (9) is the partition function for a harmonic oscillator. The rest of the quantities are written in an obvious notation.

The resonance expression, Eq. (7), has been fit to the data at 9.9 K for all three lattice-defect systems. The fitting parameters are given in Table III and the particular fit for NaCl:Cu^+ is shown in Fig. 13. The excited-state width of 6.6 cm^{-1} for NaCl:Cu^+ should be compared with the measured Raman width[13] for the E_g transition of 4.2 cm^{-1}. The difference between these two measurements is comparable with the experimental uncertainties in the far-infrared data.

From Eqs. (8) and (9) the known Li^+ concentrations in the crystals, a calculation of the transition dipole moment at 9.9 K can be made (Table III, column 5). These values are somewhat larger than the 1-Debye value [Eq. (1)] observed for P_{01} at 1.2 K. Hence, these absorption bands have roughly the correct strengths to qualify as excited-state transitions to overtone levels of the far-infrared-active resonant modes.

TABLE III. Fitting parameters for the resonant-mode excited-state transition at 9.9 K.

System	Ω_{12} (cm^{-1})	2Γ (cm^{-1})	$\Delta\epsilon$	P_{12} (debye)
KBr:^{7}LiBr	8	8	6.5×10^{-3}	1.6
KBr:^{6}LiBr	6	8	1.1×10^{-2}	1.8
NaCl:Cu^+	15	6.6	2.2×10^{-3}	

B. Paraelectric pairs

The fairly detailed identification of the resonant-mode excited state supports our earlier hypothesis and confirms that the strengths of the low-lying satellite modes vary nearly with the square of the impurity concentration. The spectrum for a 50%-50% mixture of Li^+ isotopes has not only confirmed the pair assignment but also provided a far-infrared signature of the defect center.

One possible arrangement for Li pairs would be in the form of Li_2^+ ions. Although for isotopically pure dopant this molecular ion would have no permanent dipole moment, it could undergo displasive tunneling around a normal K^+ lattice site which would produce a paraelectric spectrum similar to that observed for $KCl:^7Li^+$. The spectrum for $(^6Li\text{-}^7Li)^+$ would presumably be more complex because the molecular ion would now have a weak permanent dipole moment so that both rotational and displacive tunneling motion would be infrared active.

If Li_2^+ ions exist in the KBr lattice the center should be paramagnetic due to an unpaired $2S$ electron. Electron-spin-resonance measurements were made on a KBr crystal which had 4×10^{18} $^7Li^+/cm^3$. No ESR signal was detected with a sensitivity of 1×10^{16} spins/cm^3 for a hypothetical linewidth of 100 Gauss. To estimate the number of possible Li_2^+ centers in this sample we make use of the Thomas Reich-Kuhn sum rule to relate the line strength to the impurity concentration. By ratioing the pair spectrum strength, S_p, to the resonant-mode strength S_r, the host lattice factors drop out and one finds that

$$N_p=\frac{S_p\Omega_r\,|\,P_r\,|^2}{S_r\Omega_p\,|\,P_p\,|^2}N_r\ . \tag{10}$$

To estimate S_p we sum the strengths of the two modes given in Fig. 3(b) and for Ω_p we use the average frequency of the modes. From our measurement [Eq. (1)] $P_r\approx1$ debye while from Bridges's work,[3] $P_p\approx5$ debyes. Substituting these values into Eq. (10), we find that $N_p=2\times10^{15}$ cm^3 which is a factor of 5 smaller than the sensitivity limit of the ESR measurements. In contradiction to our earlier claim for this Li concentration,[10] our test does not eliminate the possibility that the paraelectric pair modes are caused by a diatomic lithium molecule.

Another kind of diatomic center which would produce paraelectric modes makes use of Li^+ ions in next-nearest-neighbor K^+ sites. Because of near-neighbor relaxation, each Li^+ ion would tunnel about the normal lattice equilibrium lattice site coherently with its partner. Because of the lowered symmetry along the $\langle110\rangle$ coupling axis, parallel and perpendicular modes would occur at different frequencies providing enough distinct transitions to be consistent with the complex spectra observed in Fig. 10. In order to distinguish between these two kinds of centers it will be necessary to make ESR measurements on samples with an order of magnitude larger Li concentration than those studied here.

V. CONCLUSIONS

By making far-infrared transmission measurements of KBr:LiBr and NaCl:CuCl single crystals with sample lengths an order of magnitude larger than previously used, it has been possible to identify new features of lattice-defect modes. Excited-state resonant-mode transitions are observed at frequencies far removed from those expected for a harmonic oscillator. Because of the large density of phonon states at the overtone energies, the excited-state transitions in each lattice-defect system are heavily damped with a characteristic Fröhlich resonance shape. For $KBr:Li^+$ the observed overtone shift is not consistent with that produced by a small central barrier in an otherwise harmonic potential. The shift can be accounted for with a large quartic term in the potential but such an anharmonic contribution produces a large resonant-mode Stark effect whereas only a small effect has been observed. Thus, the available data for $KBr:Li^+$ do not appear to be consistent with potential models which have been used in the past. The observed overtone shift for $NaCl:Cu^+$ is consistent with a model which contains a Fermi resonance between two nearly degenerate E_g resonant modes; however, this model is not consistent with the $KBr:Li^+$ data. Why similar excited-state spectra should require different explanations is the troublesome point which arouses fundamental questions about all of the dynamical models have been used to describe resonant-mode systems. It may be that the inconsistencies which we have identified are simply ramifications of the two configuration model—a model which appears to describe the $KI:Ag^+$ data. In order to determine whether or not this is the case more accurate temperature-dependent measurements with far-infrared and Raman spectroscopic techniques are required on all of these lattice-defect systems.

Paraelectric modes in $KBr:Li^+$ occurring far below the resonant-mode frequency have been identified with Li pairs. By monitoring the paraelectric mode strength with respect to the resonant-mode excited-state strength for a given temperature interval it has been possible to show that the paraelectric mode strength varies nearly quadratically with Li^+ concentration. The (50%-50%) Li^+ isotope mixture in KBr experiment confirms the pair mode assignment. The intriguing experimental finding is that isolated Li^+ ions do not tunnel but Li pairs do. Whether this lattice defect corresponds to a Li_2^+ molecular ion or to two next-nearest-neighbor Li^+ ions has not been resolved.

Another unusual feature of the $KBr:Li^+$ spectrum is that weak satellite modes with transitions near the resonant-mode frequency do not stem from pairs but are associated with isolated Li^+ impurities. These modes could be associated with Li complexes or Li^+ in another lattice site, e.g., an interstitial, but it is unlikely that either a complex or a different site would produce a resonant mode with nearly the same frequency as for the substitutional impurity. Recall that the $^6LiOH^-$ molecule in KBr described in Sec. III showed no strong absorption lines in this spectral region.

Finally, in long crystals of NaCl:CuCl a pair spectrum was identified at frequencies below the resonant-mode transition but no high-frequency satellites were observed. The absence of a measurable isotope splitting in this spectrum indicates that the pair modes probably are not associated with tunneling motion.

ACKNOWLEDGMENTS

Discussions with Professor F. Bridges, Professor R. Kirby, Professor F. Lüty, and Professor R. H. Silsbee have been particularly helpful. We would especially like to thank Professor Silsbee for making the ESR measurements. This work is supported in part by the U.S. Army Research Office under Grant No. DAAG-29-83-K-0044 and by the National Science Foundation under Grant No. DMR-79-24008 (Cornell University Materials Science Center Report No. 5360).

---

*Present address: Bell Communications Research, 600 Mountain Ave., Murray Hill, NJ 07974.

[1]F. Bridges, Bull. Amer. Phys. Soc. **19**, 328 (1974); F. Bridges and R. J. Russell, Solid State Commun. **21**, 1011 (1977).

[2]W. Zoller and F. Bridges, Phys. Rev. B **24**, 4796 (1981).

[3]R. J. Russell and F. Bridges, Phys. Rev. B **26**, 3386 (1982).

[4]V. Narayanamurti and R. O. Pohl, Rev. Mod. Phys. **42**, 201 (1970), and references therein.

[5]G. Lombardo and R. O. Pohl, Bull. Amer. Phys. Soc. **11**, 212 (1966).

[6]I. G. Nolt and A. J. Sievers, Phys. Rev. Lett. **16**, 1103 (1966).

[7]F. C. Baumann, J. P. Harrison, R. O. Pohl, and W. D. Seward, Phys. Rev. **159**, 691 (1967); F. C. Baumann and R. O. Pohl, *ibid.* **163**, 843 (1967).

[8]J. P. Harrison, P. P. Peressini, and R. O. Pohl, Phys. Rev. **171**, 1037 (1968).

[9]A. S. Barker and A. J. Sievers, Rev. Mod. Phys. **47**, S-2 (1975), and references therein.

[10]L. H. Greene and A. J. Sievers, Solid State Commun. **44**, 1235 (1982).

[11]A. M. Kahan, M. Patterson, and A. J. Sievers, Phys. Rev. B **14**, 5422 (1976).

[12]R. L. Blewitt and A. J. Sievers, J. Low Temp. Phys. **13**, 617 (1973).

[13]B. N. Ganguly, R. D. Kirby, M. V. Klein, and G. P. Montgomery, Phys. Rev. Lett. **28**, 307 (1972).

[14]S. A. Mabud and F. Luty, Bull. Amer. Phys. Soc. **28**, 452 (1983); F. Lüty (private communication).

[15]B. P. Clayman, R. D. Kirby, and A. J. Sievers, Phys. Rev. B **3**, 1351 (1971).

[16]A. J. Sievers and L. H. Greene, Phys. Rev. Lett. **52**, 1234 (1984).

[17]J. H. Van Vleck and V. F. Weiskopf, Rev. Mod. Phys. **17**, 227 (1945).

[18]H. Fröhlich, *Theory of Dielectric* (Clarendon, London, 1958), p. 98.

[19]C. H. Townes and A. L. Schawlow, *Microwave Spectroscopy* (McGraw-Hill, New York, 1955), Chap. 13.